ACS APPLIED MATERIALS & INTERFACES

Research Article

www.acsami.org

High-κ Lanthanum Zirconium Oxide Thin Film Dielectrics from Aqueous Solution Precursors

Keenan N. Woods,[†] Tsung-Han Chiang,[‡] Paul N. Plassmeyer,[†] Matthew G. Kast,[†] Alexander C. Lygo,[†] Aidan K. Grealish,[†] Shannon W. Boettcher,[†] and Catherine J. Page*[,†]

[†]Department of Chemistry & Biochemistry and Materials Science Institute, University of Oregon, Eugene, Oregon 97403, United States

[‡]School of Electrical Engineering and Computer Science, Oregon State University, Corvallis, Oregon 97331, United States

Supporting Information

ABSTRACT: Metal oxide thin films are critical components in modern electronic applications. In particular, high-κ dielectrics are of interest for reducing power consumption in metal−insulator−semiconductor (MIS) field-effect transistors. Although thin-film materials are typically produced via vacuum-based methods, solution deposition offers a scalable and cost-efficient alternative. We report an all-inorganic aqueous solution route to amorphous lanthanum zirconium oxide ($La_2Zr_2O_7$, LZO) dielectric thin films. LZO films were spin-cast from aqueous solutions of metal nitrates and annealed at temperatures between 300 and 600 °C to produce dense, defect-free, and smooth films with subnanometer roughness. Dielectric constants of 12.2−16.4 and loss tangents <0.6% were obtained for MIS devices utilizing LZO as the dielectric layer (1 kHz). Leakage currents <10^{-7} A cm^{-2} at 4 MV cm^{-1} were measured for samples annealed at 600 °C. The excellent surface morphology, high dielectric constants, and low leakage current densities makes these LZO dielectrics promising candidates for thin-film transistor devices.

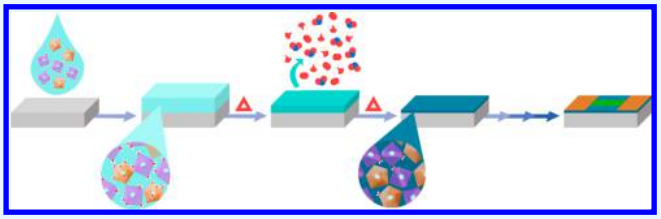

KEYWORDS: *lanthanum zirconium oxide, dielectric, aqueous solution deposition, spin-coating, thin films*

INTRODUCTION

Amorphous metal oxide thin films are used in a range of technological applications, particularly as channel and/or gate dielectric layers in metal−insulator−semiconductor field-effect transistors (MISFETs)[1] and thin-film transistors (TFTs).[2] In the case of gate components, incorporation of high-κ dielectrics into devices is attractive for reducing power consumption.[3] Zirconium oxide (ZrO_2)[4−11] and lanthanum oxide (La_2O_3)[4,12−15] are two high-κ materials (κ = 22 and 27, respectively) that have attracted interest as gate dielectric layers in MISFETs.[16] However, ZrO_2 crystallizes at relatively low annealing temperatures (~500 °C), which results in undesirable grain boundary formation, and La_2O_3 suffers from water and carbonate absorption,[17−19] both of which result in increased leakage currents and poor device properties.[20] By combining the La and Zr components into ternary lanthanum zirconium oxides, it may be possible to take advantage of the inherent high-dielectric properties while suppressing crystallization and eliminating carbonate and water absorption.

Ternary oxide phases are known for La−Zr−O,[21] and the $La_2Zr_2O_7$ crystalline pyrochlore has been extensively investigated as a substrate for epitaxial growth of YBCO superconductors.[22−29] In the past decade, amorphous $La_xZr_yO_z$ has been studied as a dielectric material and has been synthesized via vacuum-based vapor-deposition routes[30−32] and sol−gel solution-deposition routes.[33−36] Although vapor-deposition routes generally produce high-quality films,[37−40] they are energy-intensive, require expensive starting materials and equipment, and have low atom economy. In contrast, solution-deposition routes are relatively inexpensive, require less-sophisticated equipment, and can produce less waste.[41−56] However, common sol−gel routes rely on organic additives and solvents which must be expelled during film processing, leading to porosity[57] and undesirable high leakage currents in devices.[58,59] Many of these disadvantages can be circumvented by using aqueous precursors.

We report an all-inorganic, aqueous route to $La_xZr_yO_z$ (where x = 2, y = 2, and z = 7). The method employed is similar to the prompt inorganic condensation (PIC) route developed by Keszler and co-workers,[60,61] which has been used to synthesize a range of metal oxide dielectrics,[47,52,62−65] in some cases producing films that rival those deposited by vapor-phase methods.[66,67] The amorphous $La_2Zr_2O_7$ (LZO) films reported herein are smooth on a subnanometer scale and are fully condensed and densified by 600 °C. Crystallization of the LZO films does not occur until 800 °C, approximately 300 °C higher than that for pure ZrO_2. Electrical characterization of LZO-based MIS devices reveal high dielectric constants with

Received: January 18, 2017
Accepted: March 6, 2017
Published: March 6, 2017

DOI: 10.1021/acsami.7b00915
ACS Appl. Mater. Interfaces 2017, 9, 10897−10903

low deviation from ideal capacitive behavior and current density characteristics competitive with other aqueous, solution-deposited metal oxide dielectrics.[61,62,64−67]

EXPERIMENTAL METHODS

Precursor Solution Preparation. A 1.00 M (total metal, 1:1 La:Zr) LZO precursor solution was prepared by dissolving $ZrO(NO_3)_2{\cdot}xH_2O$ (Sigma-Aldrich, 99%) in 18.2 MΩ cm Millipore H_2O by gentle heating (~70 °C) and vigorous stirring of the solution. After complete dissolution, $La(NO_3)_3{\cdot}6H_2O$ (Alfa Aesar, 99.9%) was added in small portions to the still stirring solution. The solution was then diluted to 1.00 M and filtered through a 0.45 μm PTFE syringe filter.

Thin Film Preparation. Si substrates (2 × 2 cm squares) were sonicated in 5% Decon Laboratories Contrad-70 solution for 5 min and thoroughly rinsed with 18.2 MΩ cm H_2O. Substrates were then spin-dried using a spin-coater and subjected to a 1 min O_2/N_2 plasma etch using a PE-50 Benchtop Plasma Cleaner (Plasma Etch, Inc.) set to maximum power. Substrates were again rinsed with 18.2 MΩ cm H_2O and spin-dried before film deposition.

Five drops of LZO precursor solution were deposited onto cleaned Si substrates through a 0.2 μm PTFE syringe filter and then immediately spun at 3000 rpm for 30 s. Samples were directly transferred to a custom-built hot plate (consisting of an Al block with heating elements, a thermocouple, and a PID controller) set to 125 °C and ramped to a final annealing temperature of 200, 300, 400, or 500 °C at a rate of 25 °C min^{-1} and held for 1 h. Stacked, two-coat films for MIS device fabrication were annealed to 300, 400, or 500 °C for 10 min between coats and were annealed for 1 h at the desired final annealing temperature. Samples with a final annealing temperature over 500 °C were first heated to 500 °C for 10 min on the hot plate (for each layer), cooled to room temperature, and transferred to a box furnace which was ramped to the final annealing temperature (ramp rate 25 °C min^{-1}).

Precursor Solution Characterization. Samples were prepared for thermogravimetric analysis (TGA) from individual 1.0 M solutions of $ZrO(NO_3)_2{\cdot}xH_2O$, $La(NO_3)_3{\cdot}6H_2O$, and LZO precursors that were dried at 50 °C for 12 h. TGA was performed using a TA Instruments Q500A with a ramp rate of 5 °C min^{-1} under a N_2 atmosphere.

Thin Film Characterization. Fourier-transform infrared (FTIR) spectra on LZO films deposited on lightly doped double-side polished p-type Si substrates were collected using a Thermo Fisher Nicolet 6700 spectrometer. To increase the signal-to-noise ratio, FTIR analysis was performed on thicker films made from 1.8 M total metal concentration LZO precursor solutions. Background subtraction was performed by using bare Si substrates subjected to the same thermal treatment.

Grazing incidence X-ray diffraction (GIXRD) and X-ray reflectivity (XRR) analyses were conducted using a Rigaku SmartLab X-ray diffractometer (Cu Kα radiation, 40 kV, and 44 mA). X-ray reflectivity data was modeled using the BedeRefs v4.00 software package,[68] and film thicknesses and densities were extracted from the generated best fits.

Atomic force microscopy (AFM) measurements were carried out on a Digital Instruments Multimode Atomic Force Microscope with a IIIa Controller. Si tapping mode probes (Nanosensors, PPP-NCH) were used, and three measurements from different locations were taken per film over a 500 nm^2 window at a scan rate of 1 μm s^{-1}. The height and phase response were collected on the retrace sweep. After data collection, a first order flatten fit and third order plane fit was applied to remove bowing effects from the piezoelectric motors and deviations in the sample from parallel to the piezoelectric motors. NanoScope Analysis software was used to calculate the root-mean-square roughness (R_{rms}) over the area of the scan window.

Cross-sectional scanning electron microscopy (SEM) was performed using a ZEISS Ultra-55 FESEM using a 20 μm aperture and 5 kV accelerating voltage. Films were first coated in thermally evaporated Al to prevent charging effects while imaging.[69]

Device Fabrication and Testing. MIS devices were fabricated to determine LZO dielectric constants and current density−electric field characteristics (J−E). Two-coat LZO films (~100 nm) were deposited on degenerately doped p-type Si (0.008−0.020 Ω cm). Al top contacts (0.013 cm^2, ~100 nm thick) were thermally evaporated onto the stacked LZO films through a shadow mask. A back contact was made by scribing through the film to the Si substrate and applying an In/Ga eutectic. Dielectric constants were calculated from impedance measurements measured using an Agilent 4284A Precision LCR meter (20−100 000 Hz, 500 mV oscillation amplitude). Batch-to-batch variations were evaluated by making three separate samples per annealing temperature and measuring impedance of five MIS devices per sample. J−E characterization was accomplished using a Keithley 2400 SourceMeter (0.2 V steps, 0.2 s delay). J−E hysteresis tests were performed using an Agilent 4155B semiconductor parameter analyzer (0.1 V steps, 0.1 s delay). All device testing was performed in ambient atmosphere in a dark environment.

RESULTS AND DISCUSSION

The decomposition pathways of dried $La(NO_3)_3{\cdot}xH_2O$, $ZrO(NO_3)_2{\cdot}xH_2O$, and LZO precursor powders to their corresponding oxides were examined by TGA (Figure 1).

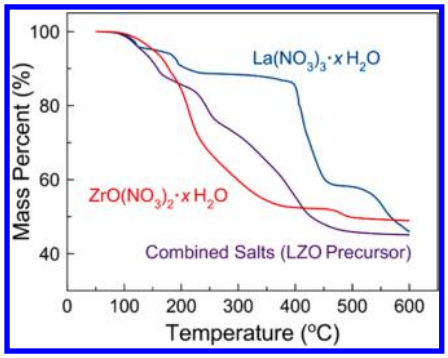

Figure 1. TGA of $La(NO_3)_3{\cdot}xH_2O$ (blue), $ZrO(NO_3)_2{\cdot}xH_2O$ (red), and LZO precursor (purple) powders derived from drying 1.0 M solutions.

Thermal decomposition of $La(NO_3)_3{\cdot}xH_2O$ begins with a small mass loss around 100 °C, likely from loss of excess (unbound) water, and proceeds through two large mass-loss events starting around 180 and 400 °C, attributable to the loss of bound water and nitrates, respectively. The final mass-loss event starting around 500 °C can be attributed to the expulsion of residual water and nitrates during the final condensation and densification of the oxide. The mass-loss profile of $ZrO(NO_3)_2{\cdot}xH_2O$ is more gradual and appears as two broad mass-loss events from 100 to 220 °C and 220 to 400 °C. These events likely correspond to gradual water and nitrate loss, respectively. The mass loss profile of the LZO precursor appears to be an approximate average of the two metal nitrate salts and shows a gradual mass decrease from 100 to 160 °C (water loss), a mass-loss event around 220 °C (nitrate loss), and a more pronounced, gradual mass loss over several hundred degrees (further nitrate loss, condensation, and film densification). Conversion of the LZO precursor to the corresponding oxide is complete by 500 °C, which occurs at a temperature lower than that for either the La or Zr nitrate salts individually. Although thermal decomposition of the bulk powders is not necessarily representative of the decomposition pathways in thin films, the bulk mass-loss events offer insight into film formation phenomena and can be related to the infrared spectroscopy conducted on thin film samples heated to various temperatures.

DOI: 10.1021/acsami.7b00915
ACS Appl. Mater. Interfaces 2017, 9, 10897−10903

FTIR spectroscopy was used to probe the hydroxide, water, and nitrate content in LZO films after annealing to various temperatures (Figure 2). Residual hydroxide and water

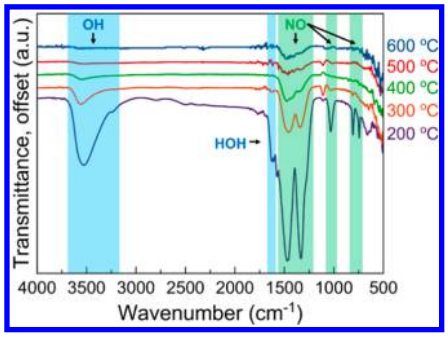

Figure 2. FTIR spectra of LZO films annealed between 200 and 600 °C.

(monitored via the broad O−H stretching mode peak around 3500 cm^{-1} and the sharp H−O−H bending mode peak around 1650 cm^{-1})[70] and NO_x content (monitored via the N−O stretches centered around 1280 and 1460 cm^{-1})[71] are dramatically reduced between 200 and 300 °C. Loss of these species is important for film stability; films annealed at or below 200 °C were not stable, absorbing water and becoming cloudy after removal from the hot plate. Due to their instability, these low-temperature annealed films were not studied by other methods and are not discussed further. By 500 °C, water and hydroxides are completely removed from the films, indicating that complete condensation has occurred. Residual NO_x appear to remain in the films up to 600 °C. The sharp peaks at 744 and 1032 cm^{-1} are present only in the spectrum for the 200 °C sample and indicate the presence of hydrated metal nitrate species.[71,72] The peak centered around 1100 cm^{-1} corresponds to Si−O−Si[73,74] vibrations and is the result of small differences in the subtraction of the sample spectra and the bare Si substrate reference.

Generally, polycrystalline films are undesirable for gate dielectrics because grain boundaries provide pathways for current leakage.[62] Amorphous films are thus preferred. GIXRD was used to assess the degree of crystallization in the films as a function of annealing temperature (Figure 3). Films remained amorphous until 800 °C, at which temperature LZO begins to crystallize as the cubic pyrochlore phase (ICSD 154752).[75] At temperatures above 1000 °C, a mixture of phases is observed.

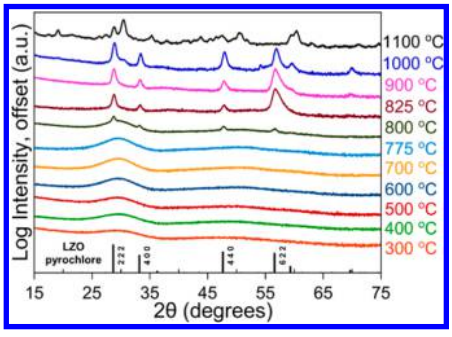

Figure 3. GIXRD of LZO films annealed between 300 and 1100 °C. LZO forms the cubic pyrochlore phase (ICSD 15475, peak positions shown in black at plot baseline) between 800 and 900 °C but decomposes at higher annealing temperatures.

The films used in MIS devices discussed below were prepared at temperatures well below the crystallization temperature (≤600 °C).

The morphology of LZO films annealed between 300 and 600 °C was examined using XRR (Figure 4a). To extract

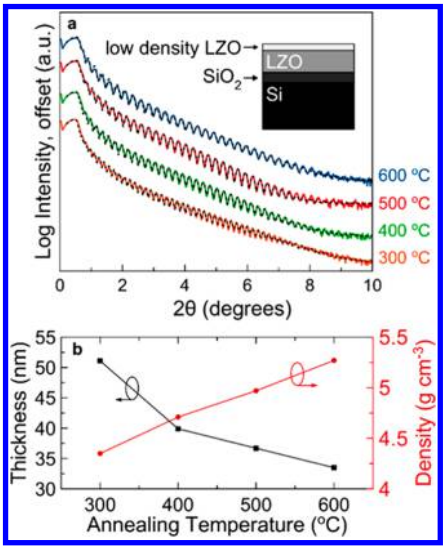

Figure 4. (a) XRR patterns of LZO films annealed between 300 and 600 °C and best-fit models (dashed, black lines). A cartoon inset depicts the two-layer model necessary for generating good fits to the data. (b) Total thickness and total density (weighted average of two-layer model) extracted from best-fit models of XRR data in panel a.

thickness, density, and surface roughness information for the LZO films, modeling of the XRR patterns was conducted using BedeRefs software.[68] Best fits were obtained using two-layer models comprised of a bulk layer and a ∼1−3 nm capping layer of different density (Figure 4, Table S1), consistent with XRR modeling performed on other aqueous solution-processed films.[76] Total film thickness decreases with increasing temperature, consistent with FTIR results, demonstrating the loss of H_2O and NO_x species as temperature increases. Overall film density (calculated from a weighted average of the densities derived from the two layer models) increases from 4.35 g cm^{-3} (300 °C) to 5.27 g cm^{-3} (600 °C), approximately 90% of the bulk density of the pyrochlore $La_2Zr_2O_7$ (6.05 g cm^{-3}).[77] Surface roughness was remarkably low (≤0.4 nm) for all samples (Figure 5b).

AFM was used to corroborate surface roughness determined from XRR modeling (Figure 5). R_{rms} values of <0.25 nm were calculated from AFM images (500 nm^2 area) of LZO films annealed between 300 and 600 °C. Film roughness decreased from 300 to 400 °C but remained constant (within error) at higher annealing temperatures. R_{rms} values determined by AFM are smaller than surface roughness values determined by XRR data modeling, which can be ascribed to differences in how AFM and XRR measurements probe the samples.[78] The subnanometer smoothness of these films makes them promising materials for a variety of electronic devices, including TFTs.[79−81]

Cross-sectional SEM was used to visualize the morphology of stacked, two-coat LZO films used in electrical device fabrication (Figure 6). The films are uniform, dense, noncrystalline, and display no signs of interfacial roughness. Film thickness

DOI: 10.1021/acsami.7b00915
ACS Appl. Mater. Interfaces 2017, 9, 10897−10903

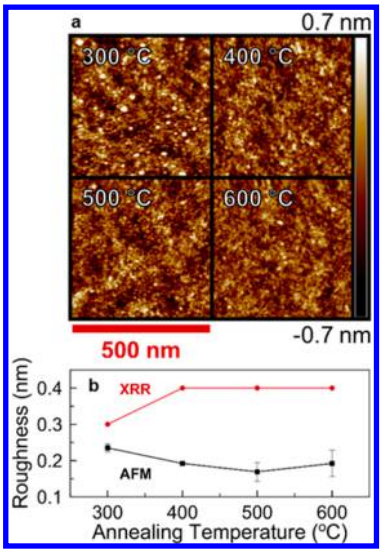

Figure 5. (a) Representative AFM images of a 500 nm^2 area and (b) comparison of surface roughness determined by XRR and AFM for LZO films annealed between 300 and 600 °C.

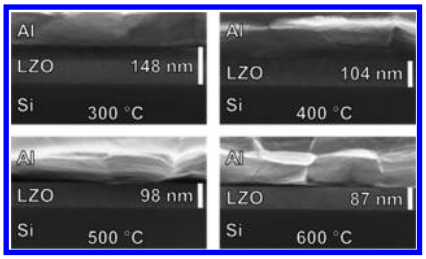

Figure 6. Cross-sectional SEM images of two-coat LZO films annealed at temperatures between 300 and 600 °C.

decreases with increasing annealing temperatures, which is in agreement with the trends observed by XRR.

The dielectric characteristics of LZO-based MIS devices were measured using impedance spectroscopy. Dielectric constants and loss tangents were measured at frequencies between 20 and 100 000 Hz (Figure S1), and dielectric constants and loss tangents measured at 1 kHz are shown in Figure 7a. The dielectric constant increases steadily with increasing annealing temperature, starting around 12.2 at 300 °C and reaching 16.4 at 600 °C. Loss tangents decrease with annealing temperature, consistent with more fully condensed (and consequently denser) films at higher annealing temperatures. Loss tangents were below 0.6% in all cases, demonstrating low deviation from ideal capacitive behavior. MIS devices were re-examined after 10 months of exposure to ambient air. Samples annealed at 300 °C showed slight decreases in dielectric constants and increased loss tangents, while films annealed ≥400 °C were stable and exhibited no change.

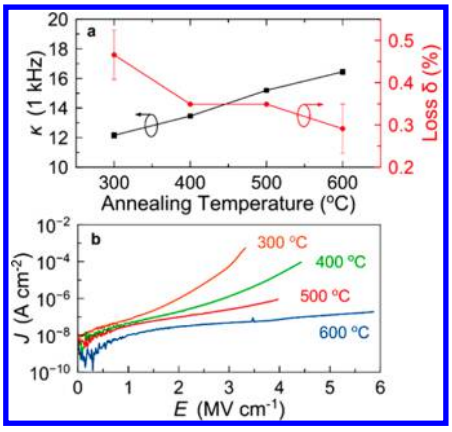

Figure 7. (a) Dielectric constants (κ) and loss tangents (loss δ) and (b) J–E data for MIS devices made from two-coat (~100 nm) LZO films.

J–E measurements were conducted to assess the effectiveness of LZO as a viable gate dielectric material (Figure 7b). Increasing the annealing temperature resulted in lower leakage currents at all electric fields. This trend is consistent with trends of decreasing water and nitrate content (FTIR), increasing film densification (XRR), and low loss tangent values. LZO MIS devices generally experienced catastrophic breakdown and loss of insulating behavior at ~4 MV cm^{-1}. Stability of the LZO devices was tested by studying J–E hysteresis of successive cycles, as shown in Figure S2. After an initial burn-in sweep, it was observed that current density settled at 10^{-7}–10^{-8} A cm^{-2}. No discernible shift was observed in J–E behavior after the second sweep, indicating good LZO dielectric stability. LZO films annealed ≥500 °C have current density characteristics that meet or exceed those of other aqueous solution-deposited dielectric materials.[61,62,64–67]

CONCLUSION

An aqueous route to high-κ lanthanum zirconium oxide dielectrics using simple nitrate salts was reported. Residual nitrate and water species are fully removed from the films by 600 °C, and the pyrochlore phase forms upon annealing to $T \geq$ 800 °C. The remarkable smoothness of these films, the high dielectric constants with low deviations from ideal capacitive behavior, and low leakage currents make them promising gate components for thin-film transistor devices. Studies examining the effects of varying La:Zr composition on film properties and toward understanding density inhomogeneities (i.e., the less dense capping layer suggested by XRR modeling) are in progress.

ASSOCIATED CONTENT

Supporting Information

The Supporting Information is available free of charge on the ACS Publications website at DOI: 10.1021/acsami.7b00915.

X-ray reflectivity best fit modeling parameters, dielectric constant dispersion data, and current–density hysteresis data (PDF)

AUTHOR INFORMATION

Corresponding Author

*E-mail: cpage@uoregon.edu.

ORCID

Shannon W. Boettcher: 0000-0001-8971-9123

Catherine J. Page: 0000-0002-4545-7835

Notes

The authors declare no competing financial interest.

ACKNOWLEDGMENTS

This work was funded by the National Science Foundation Center for Sustainable Materials Chemistry (Grant CHE-1606982). We gratefully acknowledge the use of UO

DOI: 10.1021/acsami.7b00915
ACS Appl. Mater. Interfaces 2017, 9, 10897–10903

CAMCOR High-Resolution and Nanofabrication Facility, which is supported by grants from the W. M. Keck Foundation, the M. J. Murdock Charitable Trust, ONAMI, the Air Force Research Laboratory (Agreement FA8650-05-1-5041), NSF (Awards 0923577 and 0421086), and the University of Oregon. The authors thank Prof. John Wager, Melanie Jenkins, and Fan Zhou for their valuable discussions.

REFERENCES

(1) Robertson, J. High Dielectric Constant Gate Oxides for Metal Oxide Si Transistors. *Rep. Prog. Phys.* **2006**, *69*, 327−396.
(2) Fortunato, E.; Barquinha, P.; Martins, R. Oxide Semiconductor Thin-Film Transistors: A Review of Recent Advances. *Adv. Mater.* **2012**, *24*, 2945−2986.
(3) Wilk, G. D.; Wallace, R. M.; Anthony, J. M. High-K Gate Dielectrics: Current Status and Materials Properties Considerations. *J. Appl. Phys.* **2001**, *89*, 5243−5275.
(4) Maria, J. P.; Wicaksana, D.; Kingon, A. I.; Busch, B.; Schulte, H.; Garfunkel, E.; Gustafsson, T. High Temperature Stability in Lanthanum and Zirconia-Based Gate Dielectrics. *J. Appl. Phys.* **2001**, *90*, 3476−3482.
(5) Kukli, K.; Forsgren, K.; Ritala, M.; Leskelä, M.; Aarik, J.; Hårsta, A. Dielectric Properties of Zirconium Oxide Grown by Atomic Layer Deposition from Iodide Precursor. *J. Electrochem. Soc.* **2001**, *148*, F227−F232.
(6) Adamopoulos, G.; Thomas, S.; Wöbkenberg, P. H.; Bradley, D. D. C.; McLachlan, M. A.; Anthopoulos, T. D. High-Mobility Low-Voltage ZnO and Li-Doped ZnO Transistors Based on ZrO2 High-K Dielectric Grown by Spray Pyrolysis in Ambient Air. *Adv. Mater.* **2011**, *23*, 1894−1898.
(7) Xifeng, L.; Enlong, X.; Jianhua, Z. Low-Temperature Solution-Processed Zirconium Oxide Gate Insulators for Thin-Film Transistors. *IEEE Trans. Electron Devices* **2013**, *60*, 3413−3416.
(8) Park, J. H.; Yoo, Y. B.; Lee, K. H.; Jang, W. S.; Oh, J. Y.; Chae, S. S.; Baik, H. K. Low-Temperature, High-Performance Solution-Processed Thin-Film Transistors with Peroxo-Zirconium Oxide Dielectric. *ACS Appl. Mater. Interfaces* **2013**, *5*, 410−417.
(9) Park, Y. M.; Desai, A.; Salleo, A.; Jimison, L. Solution-Processable Zirconium Oxide Gate Dielectrics for Flexible Organic Field Effect Transistors Operated at Low Voltages. *Chem. Mater.* **2013**, *25*, 2571−2579.
(10) Jang, J.; Kitsomboonloha, R.; Swisher, S. L.; Park, E. S.; Kang, H.; Subramanian, V. Transparent High-Performance Thin Film Transistors from Solution-Processed SnO2ZrO2 Gel-like Precursors. *Adv. Mater.* **2013**, *25*, 1042−1047.
(11) Liu, A.; Liu, G. X.; Zhu, H. H.; Xu, F.; Fortunato, E.; Martins, R.; Shan, F. K. Fully Solution-Processed Low-Voltage Aqueous In2O3 Thin-Film Transistors Using an Ultrathin ZrOx Dielectric. *ACS Appl. Mater. Interfaces* **2014**, *6*, 17364−17369.
(12) Yamada, H.; Shimizu, T.; Kurokawa, A.; Ishii, K.; Suzuki, E. MOCVD of High-Dielectric-Constant Lanthanum Oxide Thin Films. *J. Electrochem. Soc.* **2003**, *150*, G429−G435.
(13) He, W.; Schuetz, S.; Solanki, R.; Belot, J.; McAndrew, J. Atomic Layer Deposition of Lanthanum Oxide Films for High-κ Gate Dielectrics. *Electrochem. Solid-State Lett.* **2004**, *7*, G131−G133.
(14) Kukli, K.; Ritala, M.; Pore, V.; Leskelä, M.; Sajavaara, T.; Hegde, R. I.; Gilmer, D. C.; Tobin, P. J.; Jones, A. C.; Aspinall, H. C. Atomic Layer Deposition and Properties of Lanthanum Oxide and Lanthanum-Aluminum Oxide Films. *Chem. Vap. Deposition* **2006**, *12*, 158−164.
(15) Zhuang, J.; Sun, Q.-J.; Zhou, Y.; Han, S.-T.; Zhou, L.; Yan, Y.; Peng, H.; Venkatesh, S.; Wu, W.; Li, R. K. Y.; Roy, V. A. L. Solution-Processed Rare-Earth Oxide Thin Films for Alternative Gate Dielectric Application. *ACS Appl. Mater. Interfaces* **2016**, *8*, 31128−31135.
(16) Kingon, A. I.; Maria, J.-P.; Streiffer, S. K. Alternative Dielectrics to Silicon Dioxide for Memory and Logic Devices. *Nature* **2000**, *406*, 1032−1038.
(17) De Asha, A. M.; Critchley, J. T. S.; Nix, R. M. Molecular Adsorption Characteristics of Lanthanum Oxide Surfaces: The Interaction of Water with Oxide Overlayers Grown on Cu(111). *Surf. Sci.* **1998**, *405*, 201−214.
(18) Nieminen, M.; Putkonen, M.; Niinistö, L. Formation and Stability of Lanthanum Oxide Thin Films Deposited from β-Diketonate Precursor. *Appl. Surf. Sci.* **2001**, *174*, 155−165.
(19) Gougousi, T.; Niu, D.; Ashcraft, R. W.; Parsons, G. N. Carbonate Formation During Post-Deposition Ambient Exposure of High-K Dielectrics. *Appl. Phys. Lett.* **2003**, *83*, 3543−3545.
(20) Zhao, Y.; Toyama, M.; Kita, K.; Kyuno, K.; Toriumi, A. Moisture-Absorption-Induced Permittivity Deterioration and Surface Roughness Enhancement of Lanthanum Oxide Films on Silicon. *Appl. Phys. Lett.* **2006**, *88*, 72904.
(21) Wang, C.; Fabrichnaya, O.; Zinkevich, M.; Du, Y.; Aldinger, F. Experimental Study and Thermodynamic Modelling of the ZrO2−LaO1.5 System. *CALPHAD: Comput. Coupling Phase Diagrams Thermochem.* **2008**, *32*, 111−120.
(22) Chirayil, T. G.; Paranthaman, M.; Beach, D. B.; Lee, D. F.; Goyal, A.; Williams, R. K.; Cui, X.; Kroeger, D. M.; Feenstra, R.; Verebelyi, D. T.; Christen, D. K. Epitaxial Growth of La2Zr2O7 Thin Films on Rolled Ni-Substrates by Sol−gel Process for High Tc Superconducting Tapes. *Phys. C* **2000**, *336*, 63−69.
(23) Sathyamurthy, S.; Paranthaman, M.; Aytug, T.; Kang, B. W.; Martin, P. M.; Goyal, A.; Kroeger, D. M.; Christen, D. K. Chemical Solution Deposition of Lanthanum Zirconate Buffer Layers on Biaxially Textured Ni−1.7% Fe−3% W Alloy Substrates for Coated-Conductor Fabrication. *J. Mater. Res.* **2002**, *17*, 1543−1549.
(24) Sathyamurthy, S.; Paranthaman, M.; Zhai, H.-Y.; Christen, H. M.; Martin, P. M.; Goyal, A. Lanthanum Zirconate: A Single Buffer Layer Processed by Solution Deposition for Coated Conductor Fabrication. *J. Mater. Res.* **2002**, *17*, 2181−2184.
(25) Knoth, K.; Schlobach, B.; Hühne, R.; Schultz, L.; Holzapfel, B. La2Zr2O7 and Ce−Gd−O Buffer Layers for YBCO Coated Conductors Using Chemical Solution Deposition. *Phys. C* **2005**, *426−431*, 979−984.
(26) Sathyamurthy, S.; Paranthaman, M.; Heatherly, L.; Martin, P. M.; Specht, E. D.; Goyal, A.; Kodenkandath, T.; Li, X.; Rupich, M. W. Solution-Processed Lanthanum Zirconium Oxide as a Barrier Layer for High Ic-Coated Conductors. *J. Mater. Res.* **2006**, *21*, 910−914.
(27) Jin, L.; Yu, Z.; Zhang, Y.; Wang, Y.; Yan, G.; Li, C.; Lu, Y. Effect of La2Zr2O7-Buffered YSZ Substrate on YBa2Cu3Oy Thin Films by Chemical Solution Deposition. *Phys. C* **2010**, *470*, 602−605.
(28) Chen, H. S.; Kumar, R. V.; Glowacki, B. A. Chemical Solution Deposited Lanthanum Zirconium Oxide Thin Films: Synthesis and Chemistry. *Mater. Chem. Phys.* **2010**, *122*, 305−310.
(29) Molina-Luna, L.; Egoavil, R.; Turner, S.; Thersleff, T.; Verbeeck, J.; Holzapfel, B.; Eibl, O.; Van Tendeloo, G. Interlayer Structure in YBCO-Coated Conductors Prepared by Chemical Solution Deposition. *Supercond. Sci. Technol.* **2013**, *26*, 75016.
(30) Gaskell, J. M.; Jones, A. C.; Aspinall, H. C.; Taylor, S.; Taechakumput, P.; Chalker, P. R.; Heys, P. N.; Odedra, R. Deposition of Lanthanum Zirconium Oxide High-K Films by Liquid Injection Atomic Layer Deposition. *Appl. Phys. Lett.* **2007**, *91*, 112912.
(31) Gaskell, J. M.; Jones, A. C.; Chalker, P. R.; Werner, M.; Aspinall, H. C.; Taylor, S.; Taechakumput, P.; Heys, P. N. Deposition of Lanthanum Zirconium Oxide High-K Films by Liquid Injection ALD and MOCVD. *Chem. Vap. Deposition* **2007**, *13*, 684−690.
(32) Alessandri, M.; Del Vitto, A.; Piagge, R.; Sebastiani, A.; Scozzari, C.; Wiemer, C.; Lamagna, L.; Perego, M.; Ghidini, G.; Fanciulli, M. Rare Earth-Based High-K Materials for Non-Volatile Memory Applications. *Microelectron. Eng.* **2010**, *87*, 290−293.
(33) Tue, P. T.; Li, J.; Miyasako, T.; Inoue, S.; Shimoda, T. Low-Temperature All-Solution-Derived Amorphous Oxide Thin-Film Transistors. *IEEE Electron Device Lett.* **2013**, *34*, 1536−1538.
(34) Tue, P. T.; Miyasako, T.; Li, J.; Tu, H. T. C.; Inoue, S.; Tokumitsu, E.; Shimoda, T. High-Performance Solution-Processed ZrInZnO Thin-Film Transistors. *IEEE Trans. Electron Devices* **2013**, *60*, 320−326.

DOI: 10.1021/acsami.7b00915
ACS Appl. Mater. Interfaces 2017, 9, 10897−10903

(35) Je, S. Y.; Son, B.-G.; Kim, H.-G.; Park, M.-Y.; Do, L.-M.; Choi, R.; Jeong, J. K. Solution-Processable LaZrOx/SiO2 Gate Dielectric at Low Temperature of 180 °C for High-Performance Metal Oxide Field-Effect Transistors. *ACS Appl. Mater. Interfaces* **2014**, *6*, 18693−18703.
(36) Li, J.; Zhu, P.; Hirose, D.; Kohara, S.; Shimoda, T. Hybrid Cluster Precursors of the LaZrO Insulator for Transistors: Properties of High-Temperature-Processed Films and Structures of Solutions, Gels, and Solids. *Sci. Rep.* **2016**, *6*, 29682.
(37) Niinistö, L.; Päiväsaari, J.; Niinistö, J.; Putkonen, M.; Nieminen, M. Advanced Electronic and Optoelectronic Materials by Atomic Layer Deposition: An Overview with Special Emphasis on Recent Progress in Processing of High-K Dielectrics and Other Oxide Materials. *Phys. Status Solidi A* **2004**, *201*, 1443−1452.
(38) Jones, A. C.; Aspinall, H. C.; Chalker, P. R.; Potter, R. J.; Kukli, K.; Rahtu, A.; Ritala, M.; Leskela, M. Some Recent Developments in the MOCVD and ALD of High-K Dielectric Oxides. *J. Mater. Chem.* **2004**, *14*, 3101−3112.
(39) Jones, A. C.; Chalker, P. R. Some Recent Developments in the Chemical Vapour Deposition of Electroceramic Oxides. *J. Phys. D: Appl. Phys.* **2003**, *36*, R80−R95.
(40) Christen, H. M.; Eres, G. Recent Advances in Pulsed-Laser Deposition of Complex Oxides. *J. Phys.: Condens. Matter* **2008**, *20*, 264005.
(41) Ong, B. S.; Li, C.; Li, Y.; Wu, Y.; Loutfy, R. Stable, Solution-Processed, High-Mobility ZnO Thin-Film Transistors. *J. Am. Chem. Soc.* **2007**, *129*, 2750−2751.
(42) Jeong, Y.; Kim, D.; Song, K.; Jun, T.; Woo, K.; Moon, J. Solution-Processed Stable Zinc Oxide Semiconductor for Thin-Film Transistors. *J. Phys. Chem. C* **2008**, *112*, 11082−11085.
(43) Pal, B. N.; Trottman, P.; Sun, J.; Katz, H. E. Solution-Deposited Zinc Oxide and Zinc Oxide/Pentacene Bilayer Transistors: High Mobility N-Channel, Ambipolar, and Nonvolatile Devices. *Adv. Funct. Mater.* **2008**, *18*, 1832−1839.
(44) Meyers, S. T.; Anderson, J. T.; Hung, C. M.; Thompson, J.; Wager, J. F.; Keszler, D. A. Aqueous Inorganic Inks for Low-Temperature Fabrication of ZnO TFTs. *J. Am. Chem. Soc.* **2008**, *130*, 17603−17609.
(45) Adamopoulos, G.; Bashir, A.; Gillin, W. P.; Georgakopoulos, S.; Shkunov, M.; Baklar, M. A.; Stingelin, N.; Bradley, D. D. C.; Anthopoulos, T. D. Structural and Electrical Characterization of ZnO Films Grown by Spray Pyrolysis and Their Application in Thin-Film Transistors. *Adv. Funct. Mater.* **2011**, *21*, 525−531.
(46) Thomas, S. R.; Pattanasattayavong, P.; Anthopoulos, T. D. Solution-Processable Metal Oxide Semiconductors for Thin-Film Transistor Applications. *Chem. Soc. Rev.* **2013**, *42*, 6910−6923.
(47) Jiang, K.; Meyers, S. T.; Anderson, M. D.; Johnson, D. C.; Keszler, D. A. Functional Ultrathin Films and Nanolaminates from Aqueous Solutions. *Chem. Mater.* **2013**, *25*, 210−214.
(48) Xu, W.; Wang, H.; Ye, L.; Xu, J. The Role of Solution-Processed High-K Gate Dielectrics in Electrical Performance of Oxide Thin-Film Transistors. *J. Mater. Chem. C* **2014**, *2*, 5389−5396.
(49) Esro, M.; Vourlias, G.; Somerton, C.; Milne, W. I.; Adamopoulos, G. High-Mobility ZnO Thin Film Transistors Based on Solution-Processed Hafnium Oxide Gate Dielectrics. *Adv. Funct. Mater.* **2015**, *25*, 134−141.
(50) Xu, W.; Cao, H.; Liang, L.; Xu, J.-B. Aqueous Solution-Deposited Gallium Oxide Dielectric for Low-Temperature, Low-Operating-Voltage Indium Oxide Thin-Film Transistors: A Facile Route to Green Oxide Electronics. *ACS Appl. Mater. Interfaces* **2015**, *7*, 14720−14725.
(51) Liu, G.; Liu, A.; Zhu, H.; Shin, B.; Fortunato, E.; Martins, R.; Wang, Y.; Shan, F. Low-Temperature, Nontoxic Water-Induced Metal-Oxide Thin Films and Their Application in Thin-Film Transistors. *Adv. Funct. Mater.* **2015**, *25*, 2564−2572.
(52) Nadarajah, A.; Wu, M. Z. B.; Archila, K.; Kast, M. G.; Smith, A. M.; Chiang, T. H.; Keszler, D. A.; Wager, J. F.; Boettcher, S. W. Amorphous In−Ga−Zn Oxide Semiconducting Thin Films with High Mobility from Electrochemically Generated Aqueous Nanocluster Inks. *Chem. Mater.* **2015**, *27*, 5587−5596.
(53) Esro, M.; Mazzocco, R.; Vourlias, G.; Kolosov, O.; Krier, A.; Milne, W. I.; Adamopoulos, G. Solution Processed Lanthanum Aluminate Gate Dielectrics for Use in Metal Oxide-Based Thin Film Transistors. *Appl. Phys. Lett.* **2015**, *106*, 203507.
(54) Xu, W.; Wang, H.; Xie, F.; Chen, J.; Cao, H.; Xu, J.-B. Facile and Environmentally Friendly Solution-Processed Aluminum Oxide Dielectric for Low-Temperature, High-Performance Oxide Thin-Film Transistors. *ACS Appl. Mater. Interfaces* **2015**, *7*, 5803−5810.
(55) Liu, A.; Liu, G.; Zhu, H.; Song, H.; Shin, B.; Fortunato, E.; Martins, R.; Shan, F. Water-Induced Scandium Oxide Dielectric for Low-Operating Voltage N- and P-Type Metal-Oxide Thin-Film Transistors. *Adv. Funct. Mater.* **2015**, *25*, 7180−7188.
(56) Park, S.; Kim, C.-H.; Lee, W.-J.; Sung, S.; Yoon, M.-H. Sol-Gel Metal Oxide Dielectrics for All-Solution-Processed Electronics. *Mater. Sci. Eng., R* **2017**, *114*, 1−22.
(57) Brinker, C. J.; Scherer, G. W. *Sol-Gel Science: The Physics and Chemsistry of Sol-Gel Processing*; Academic Press: San Diego, CA, 1990.
(58) Fan, Q.; McQuillin, B.; Ray, A. K.; Turner, M. L.; Seddon, A. B. High Density, Non-Porous Anatase Titania Thin Films for Device Applications. *J. Phys. D: Appl. Phys.* **2000**, *33*, 2683−2686.
(59) Wang, Z.; Helmersson, U.; Käll, P.-O. Optical Properties of Anatase TiO2 Thin Films Prepared by Aqueous Sol−Gel Process at Low Temperature. *Thin Solid Films* **2002**, *405*, 50−54.
(60) Anderson, J. T.; Munsee, C. L.; Hung, C. M.; Phung, T. M.; Herman, G. S.; Johnson, D. C.; Wager, J. F.; Keszler, D. A. Solution-Processed HafSOx and ZircSOx Inorganic Thin-Film Dielectrics and Nanolaminates. *Adv. Funct. Mater.* **2007**, *17*, 2117−2124.
(61) Meyers, S. T.; Anderson, J. T.; Hong, D.; Hung, C. M.; Wager, J. F.; Keszler, D. A. Solution-Processed Aluminum Oxide Phosphate Thin-Film Dielectrics. *Chem. Mater.* **2007**, *19*, 4023−4029.
(62) Jiang, K.; Anderson, J. T.; Hoshino, K.; Li, D.; Wager, J. F.; Keszler, D. A. Low-Energy Path to Dense HfO2 Thin Films with Aqueous Precursor. *Chem. Mater.* **2011**, *23*, 945−952.
(63) Alemayehu, M.; Davis, J. E.; Jackson, M.; Lessig, B.; Smith, L.; Sumega, J. D.; Knutson, C.; Beekman, M.; Johnson, D. C.; Keszler, D. A. Tunable Dielectric Thin Films by Aqueous, Inorganic Solution-Based Processing. *Solid State Sci.* **2011**, *13*, 2037−2040.
(64) Plassmeyer, P. N.; Archila, K.; Wager, J. F.; Page, C. J. Lanthanum Aluminum Oxide Thin-Film Dielectrics from Aqueous Solution. *ACS Appl. Mater. Interfaces* **2015**, *7*, 1678−1684.
(65) Norelli, K. M.; Plassmeyer, P. N.; Woods, K. N.; Glassy, B. A.; Knutson, C. C.; Beekman, M.; Page, C. J. Influence of Composition and Processing Parameters on the Properties of Solution-Processed Aluminum Phosphate Oxide (AlPO) Thin Tilms. *Solid State Sci.* **2016**, *55*, 8−12.
(66) Kim, K. M.; Kim, C. W.; Heo, J. S.; Na, H.; Lee, J. E.; Park, C. B.; Bae, J.-U.; Kim, C.-D.; Jun, M.; Hwang, Y. K.; Meyers, S. T.; Grenville, A.; Keszler, D. A. Competitive Device Performance of Low-Temperature and All-Solution-Processed Metal-Oxide Thin-Film Transistors. *Appl. Phys. Lett.* **2011**, *99*, 242109.
(67) Smith, S. W.; Wang, W.; Keszler, D. A.; Conley, J. F. Solution Based Prompt Inorganic Condensation and Atomic Layer Deposition of Al2O3 Films: A Side-by-Side Comparison. *J. Vac. Sci. Technol., A* **2014**, *32*, 41501.
(68) Wormington, M.; Panaccione, C.; Matney, K. M.; Bowen, D. K. Characterization of Structures from X-Ray Scattering Data Using Genetic Algorithms. *Philos. Trans. R. Soc., A* **1999**, *357*, 2827−2848.
(69) Kim, K. H.; Akase, Z.; Suzuki, T.; Shindo, D. Charging Effects on SEM/SIM Contrast of Metal/Insulator System in Various Metallic Coating Conditions. *Mater. Trans.* **2010**, *51*, 1080−1083.
(70) Al-Abadleh, H. A.; Grassian, V. H. FT-IR Study of Water Adsorption on Aluminum Oxide Surfaces. *Langmuir* **2003**, *19*, 341−347.
(71) Nyquist, R. A.; Putzig, C. L.; Leugers, M. A.; Kagel, R. O. *The Handbook of Infrared and Raman Spectra of Inorganic Compounds and Organic Salts*; Academic Press: San Diego, CA, 1997.
(72) Klingenberg, B.; Vannice, M. A. Influence of Pretreatment on Lanthanum Nitrate, Carbonate, and Oxide Powders. *Chem. Mater.* **1996**, *8*, 2755−2768.

DOI: 10.1021/acsami.7b00915
ACS Appl. Mater. Interfaces 2017, 9, 10897−10903

(73) Martinet, C.; Devine, R. A. B. Analysis of the Vibrational Mode Spectra of Amorphous SiO2 Films. *J. Appl. Phys.* **1995**, *77*, 4343−4348.
(74) Devine, R. A. B. Structural Nature of the Si/SiO2 Interface Through Infrared Spectroscopy. *Appl. Phys. Lett.* **1996**, *68*, 3108−3110.
(75) Uno, M.; Kosuga, A.; Okui, M.; Horisaka, K.; Muta, H.; Kurosaki, K.; Yamanaka, S. Photoelectrochemical Study of Lanthanide Zirconium Oxides, Ln2Zr2O7 (Ln = La, Ce, Nd and Sm). *J. Alloys Compd.* **2006**, *420*, 291−297.
(76) Fairley, K. C.; Merrill, D. R.; Woods, K. N.; Ditto, J.; Xu, C.; Oleksak, R. P.; Gustafsson, T.; Johnson, D. W.; Garfunkel, E. L.; Herman, G. S.; Johnson, D. C.; Page, C. J. Non-Uniform Composition Profiles in Inorganic Thin Films from Aqueous Solutions. *ACS Appl. Mater. Interfaces* **2016**, *8*, 667−672.
(77) Yugeswaran, S.; Selvarajan, V.; Ananthapadmanabhan, P. V.; Lusvarghi, L. Twin Step Synthesis of Lanthanum Zirconate Through Transferred Arc Plasma Processing. *J. Phys. Conf. Ser.* **2010**, *208*, 12119.
(78) Kojima, I.; Li, B. Structural Characterization of Thin Films by X-Ray. *Rigaku J.* **1999**, *16*, 31−42.
(79) Jung, Y.; Kline, R. J.; Fischer, D. A.; Lin, E. K.; Heeney, M.; McCulloch, I.; DeLongchamp, D. M. The Effect of Interfacial Roughness on the Thin Film Morphology and Charge Transport of High-Performance Polythiophenes. *Adv. Funct. Mater.* **2008**, *18*, 742−750.
(80) Lee, J.-M.; Choi, B.-H.; Ji, M.-J.; Park, J.-H.; Kwon, J.-H.; Ju, B.-K. The Improved Performance of a Transparent ZnO Thin-Film Transistor with AlN/Al2O3 Double Gate Dielectrics. *Semicond. Sci. Technol.* **2009**, *24*, 55008.
(81) Alimardani, N.; Cowell, E. W., III; Wager, J. F.; Conley, J. F., Jr.; Evans, D. R.; Chin, M.; Kilpatrick, S. J.; Dubey, M. Impact of Electrode Roughness on Metal-Insulator-Metal Tunnel Diodes with Atomic Layer Deposited Al2O3 Tunnel Barriers. *J. Vac. Sci. Technol., A* **2012**, *30*, 01A113.

DOI: 10.1021/acsami.7b00915
ACS Appl. Mater. Interfaces 2017, 9, 10897−10903